Acta Crystallographica Section D
Biological Crystallography
ISSN 0907-4449

Structure determination of bacteriophage PP7 from *Pseudomonas aeruginosa*: from poor data to a good map

Kaspars Tars,[a] Kerstin Fridborg,[a] Maija Bundule[b] and Lars Liljas[a]*

[a]Department of Cell and Molecular Biology, Uppsala University, Box 596, S751 24 Uppsala, Sweden, and [b]Biomedical Research and Study Centre, Ratsupites 1, LV 1067, Riga, Latvia

Correspondence e-mail: lars@alpha2.bmc.uu.se

Received 14 May 1999
Accepted 21 January 2000

PDB Reference: bacteriophage PP7, 1dwn.

The structure of bacteriophage PP7 from *Pseudomomas aeruginosa* was determined to 3.7 Å resolution. Triclinic crystals of three forms were obtained, diffracting to between 4.5 and 3.4 Å resolution. The quality of the crystals was exceptionally poor, leading to problems in the evaluation of the recorded images and to a final data set which would appear to be useless with standard criteria for protein crystals. In all crystal forms, the unit cell contains two icosahedral particles, providing 120-fold non-crystallographic symmetry. For two of the crystal forms, the particle orientations were calculated using the self-rotation function. The two particles in the asymmetric unit had very similar but distinct orientations. The position of the second particle was found using the Patterson function. Initial phases to 15 Å resolution were calculated using the related phage MS2 as a model. Real-space averaging was performed and phases were extended from 15 Å resolution to the limit of the data. The map was improved significantly by using only the 'high' resolution data in the resolution range 7–3.7 Å, allowing the positions of most side chains to be determined. The better quality of the 7–3.7 Å resolution map is presumably a consequence of the presence of satellite crystals. The position of the second particle was improved using the correlation coefficient in the averaging process to monitor the refinement by moving the particle around in small steps.

1. Introduction

Methods for the structure determination of viruses are well established. Initial phases to relatively low resolution can be extended to a resolution where an atomic model can be built in the electron-density map (Hogle *et al.*, 1985; Rossmann *et al.*, 1985). The initial phases are obtained from isomorphous replacement or molecular replacement. For molecular replacement, models of distantly related viruses (Hogle *et al.*, 1986; Luo *et al.*, 1987; Acharya *et al.*, 1989; Golmohammadi *et al.*, 1996; Chandrasekar & Johnson, 1998; Tate *et al.*, 1999) or even still simpler models (Valegård *et al.*, 1991; McKenna *et al.*, 1992; Speir *et al.*, 1995; Simpson *et al.*, 1998; Munshi *et al.*, 1998; Dokland *et al.*, 1998) have been used. The phase extension requires accurate parameters for the orientation and position of particles.

P. aeruginosa phage PP7 is related to small RNA coliphages such as MS2 (Valegård *et al.*, 1990; Golmohammadi *et al.*, 1993), GA (Tars *et al.*, 1997) and Qβ (Golmohammadi *et al.*, 1996). It has a $T = 3$ shell composed of 180 chemically identical monomers, each 127 amino-acid residues in length. Additionally, there is a single copy of the A protein per virion. The positive-stranded RNA genome (3588 nucleotides) also codes for the replicase and lysis proteins (Olsthoorn *et al.*, 1995). The

presence of a further protein, called p25, has been reported (Olsthoorn *et al.*, 1995), but its origin is not clear. The N-terminal amino-acid sequence of p25 is identical to that of coat protein. The molecular weight of p25 is incompatible with any read-through or ribosome frameshift model. The current explanation is that p25 might be a covalently associated dimer of the normal coat protein.

Here, we report the crystallization and structure determination of phage PP7 to 3.7 Å resolution using the molecular-replacement method. In this case, no model with significant sequence similarities is available, but PP7 was assumed to be similar to MS2 and other coliphages because of the similarity in the genome organization. The special problems encountered in this case were the poor quality of the crystals and the large number of parameters to be determined in the *P*1 cell containing two particles with very similar orientations.

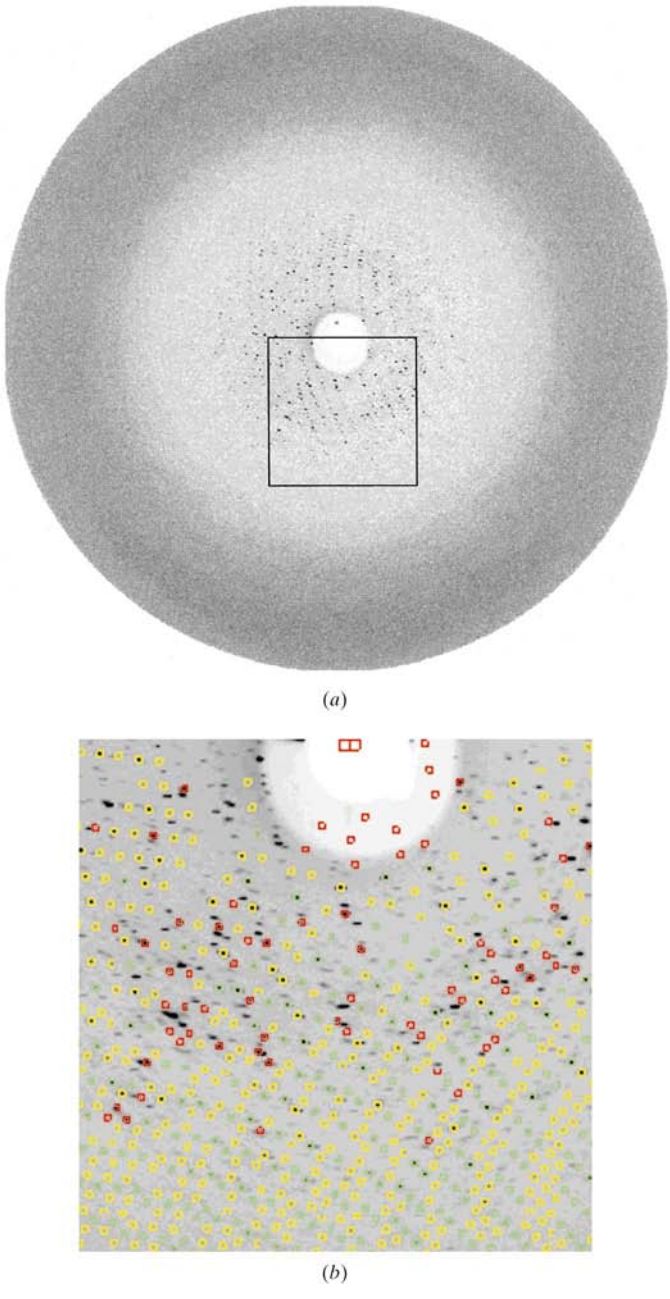

Figure 1
(*a*) The diffraction pattern of a PP7 crystal (form *B*, oscillation angle 0.5°). The enlarged plot (*b*) also shows the predicted pattern by *DENZO*, defined by the final parameters from the post-refinement. Many spots are found which are not predicted, especially at very low resolution, which might be caused by the crystal aggregation.

Table 1
Unit-cell dimensions for the three crystal forms.

	Crystal form *A*	Crystal form *B*	Crystal form *C*
a (Å)	284	285	283
b (Å)	328	324	340
c (Å)	365	380	392
α (°)	90.5	88.4	83.6
β (°)	91.0	88.1	82.4
γ (°)	89.0	87.7	81.1

2. Methods

P. aeruginosa strain PA01 cells were grown in a rich 2TY medium (1.6% tryptone, 1% yeast extract and 0.5% NaCl) to a density of 6×10^8 bacteria ml^{-1}, infected with phage PP7 at a multiplicity of 10 and incubated for another 4 h. After removal of cell debris by centrifugation, the phage was precipitated with dry ammonium sulfate to 40% saturation, centrifuged, dissolved in 20 m*M* Tris–HCl buffer pH 8.0 and applied to a Sepharose CL-4B gel-filtration column. Peak fractions were collected, precipitated and applied two more times to the same column. Fractions from the final separation were examined on polyacrylamide–SDS gel, precipitated with 10% PEG 6000 and dissolved in 20 m*M* Tris–HCl buffer pH 8.0. Besides the major PP7 coat-protein band, thin bands corresponding to the molecular weight of the A protein and the p25 protein were observed on the SDS gel. Depending on the individual phage preparations, the amount of p25 varied from 1 to 10% of the total capsid material as crudely estimated from the band intensity on the gel. When the concentration of p25 was high (5–10%), the protein solution was coloured red as described by Olsthoorn *et al.* (1995). Useful crystals were never obtained from red preparations. This might be because of an enhanced asymmetry of particles caused by the presence of several p25 protein molecules on the capsid surface. The phage particle also contains a single copy of the A protein, which might cause additional asymmetry of the capsid.

Crystals were obtained under two different conditions using the hanging-drop technique. In both cases, 5 µl of phage solution (7 mg ml^{-1}) was mixed with an equal volume of reservoir solution. Crystal type *A* (irregular shape) was obtained using 0.2 *M* magnesium acetate, 0.1 *M* sodium cacodylate pH 6.5 and 30%(*v*/*v*) 2-methyl-4,4-pentanediol at room temperature. Crystal types *B* and *C* (rhombic shape) were obtained using 0.1 *M* sodium citrate buffer pH 5.6 and 3.0 *M* 1,6-hexanediol at 310 K. Crystal form *A* grew to a maximum dimension of 1 mm in about two weeks. Crystal forms *B* and *C* grew to a size of 1.8 mm in about six weeks.

Data was collected on a MAR 30 image plate and ADSC Quantum 4 CCD detectors at station 9.6 of the SERC

Synchrotron Radiation Source in Daresbury, England and on a MAR 30 image plate at the MAX-Lab synchrotron facility in Lund, Sweden. Data was processed and scaled with the *HKL* package (Otwinowski & Minor, 1996). Data for crystal form *A* were merged using the *HKL* package with no rejections. Data for crystal forms *B* and *C* were merged using the *CCP*4 program *AGROVATA* (Collaborative Computational Project, Number 4, 1994). For crystal form *B*, less than 0.3% of the measurements (0.7% of the scaling reflections) were rejected using the default rejection criteria in *AGROVATA*. No σ cutoff was used. In this data set, the fractional bias was estimated to be about 8%. In the final merging using *AGROVATA*, partial reflections recorded on adjacent images were added to the equivalent full reflections. Of the remaining partial reflections not recorded on adjacent images, those that were more than 50% recorded on one image were used and

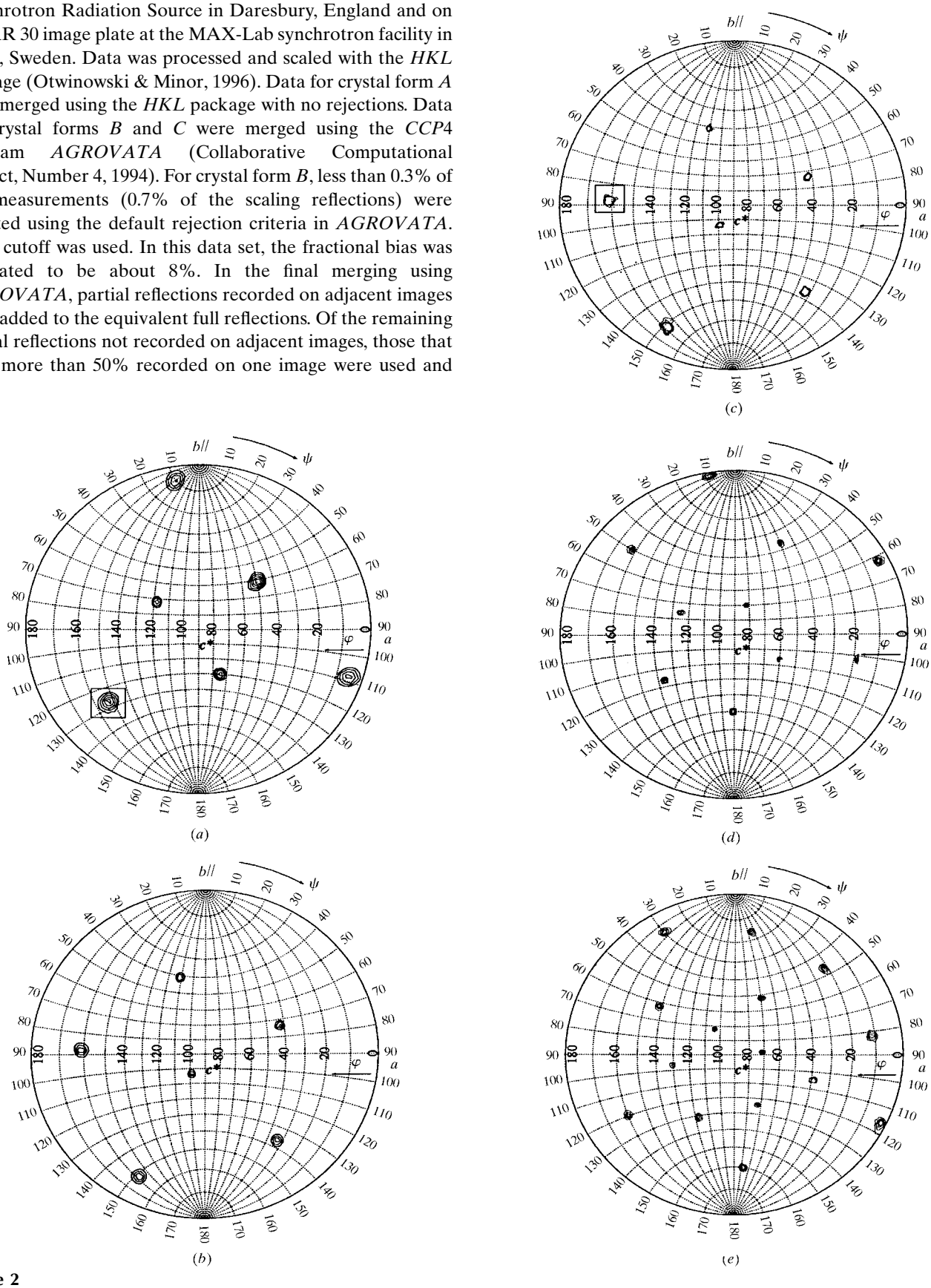

Figure 2
Rotation functions of the crystal forms *A* and *B*. (*a*) Crystal form *A*, $\kappa = 72^\circ$, 10–4.3 Å resolution; (*b*) crystal form *B*, $\kappa = 72^\circ$, 10–3.4 Å resolution; (*c*) crystal form *B*, $\kappa = 72^\circ$, 4.5–3.4 Å resolution. Note that the peaks have a tendency to splitting when compared with (*b*). (*d*) Crystal form *B*, $\kappa = 120^\circ$, 10–3.4 Å resolution; (*e*) crystal form *B*, $\kappa = 180^\circ$, 10–3.4 Å resolution.

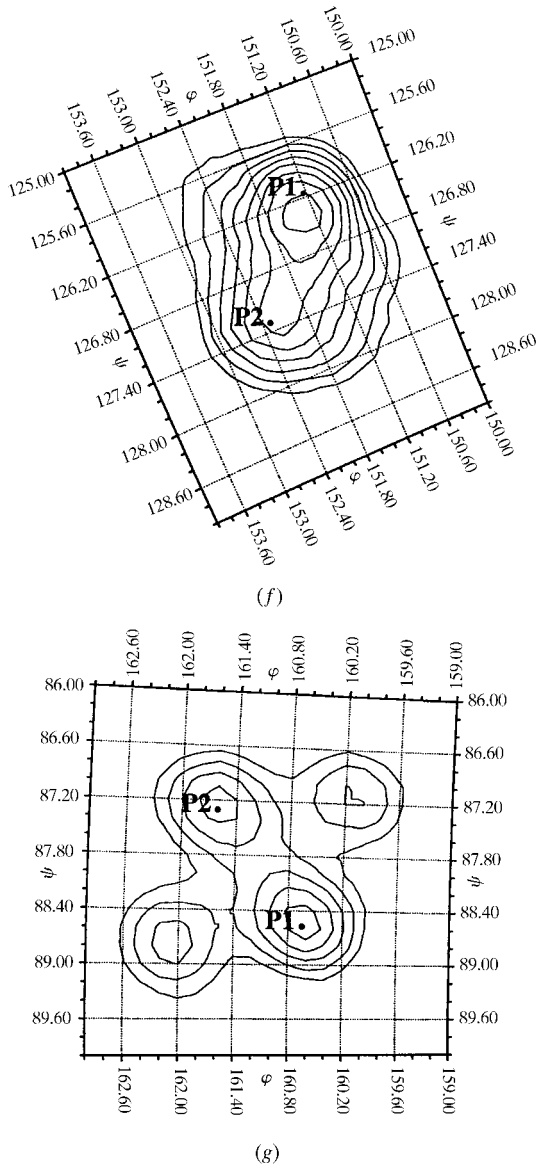

Figure 2 (continued)
(*f*) Crystal form *A*, close-up view of one fivefold peak [marked with a square in (*a*)], 5.5–4.4 Å resolution; (*g*) crystal form *B*, close-up view of one fivefold peak [marked with a square in (*c*)], 4.5–3.4 Å resolution. True peaks corresponding to different particle orientations are marked with P1 and P2.

their intensities were divided by their degree of partiality estimated in *DENZO*.

The self-rotation function was calculated using the program *GLRF* (Rossmann & Blow, 1962; Tong & Rossmann, 1990).

3. Results and discussion

3.1. Data collection and processing

In total, about 20 crystals of form *A* and about 20 crystals of form *B* were used. An oscillation angle of 0.4 or 0.5° was used. Crystal form *A* appeared to be sensitive to radiation damage. The maximal resolution (4.3 Å) could be recorded only on the first image. Crystal form *B* (not available from the beginning) was somewhat less sensitive to radiation and the maximal resolution was 3.4 Å. However, higher resolution data (beyond 4.5 Å) was weak. From three to ten images were obtained from each position of the crystal.

The $\langle I/\sigma(I)\rangle$ ratio from *DENZO* was used to determine the individual resolution limit for each image. The maximal resolution with $\langle I/\sigma(I)\rangle > 2$ was used. The quality of the crystals within a single crystal form was similar, but some were small and could be used only to low resolution. The diffraction pattern at low resolution was very complex, which made the autoindexing unusually difficult. As shown in Fig. 1, many strong spots at low resolution were not part of the predicted pattern. One explanation might be that the crystals were an aggregate containing one major crystal and several smaller satellite crystals. However, some crystals seemed regular, but still showed the same complex diffraction pattern. We were not able to find a procedure for autoindexing that would work for most crystals. For each crystal, different combinations of high- and low-resolution limits, spot size and number of spots were tested until the correct indexing was found. We never managed to index some crystals. The correctness of the solution could be identified by the similarities of the unit-cell parameters to the established parameters for that crystal type and by the relative similarity of the predicted and observed spot positions at high resolution. The identification of a correct indexing was further complicated by the fact that the similar crystal forms *B* and *C* were obtained using the same conditions and did not differ in morphology. In all three crystal forms, the space group is *P*1 with angles close to 90° (Table 1).

Since the unit-cell angles are close to 90°, the autoindexing did not always choose a unit cell with the same axis direction. Therefore, the reflections from each crystal had to be scaled to a small data set of consistently indexed reflections to ensure the correct choice of the axis directions. The four possible ways of indexing were tried by applying a re-indexing matrix in *SCALEPACK*. The χ^2 values were always much lower for the correct indexing.

After scaling and post-refinement, all images were reprocessed using the refined unit-cell dimensions (which were fixed) and the properly transformed mis-setting angles. For some images, the unit-cell parameters obtained after autoindexing and refinement in *DENZO* differed significantly from the parameters from post-refinement. Reprocessing of these images often required a stepwise change in the unit-cell parameters combined with refinement until the final parameters were reached. Reprocessing with the correct cell gave more reflections and better scaling statistics. The crystal mosaicity was determined from the profiles of the average intensities of partial reflections in *DENZO*. Values between 0.2 and 0.4° were obtained. In some cases, the mosaicity appeared to be still higher, but scaling of data from images with no full reflections did not work well. No post-refinement was performed in the final scaling. The unit-cell parameters were redetermined using the reprocessed data. The small amount of data available did not allow a separate refinement of the unit-cell parameters for each crystal.

Statistics from the scaling of crystal forms *A* and *B* are shown in Table 2. The multiplicity was 1.3 and 1.4, respectively, for these two data sets. Of the measurements used, 19 and 24% were full reflections for crystal forms *A* and *B*, respectively. *R* factors for the higher resolution data (below 6 Å) were very high. The resulting data was still useful, as demonstrated by the rotation function below. Data for crystal form *C* was too incomplete to be used for further calculations.

3.2. Packaging of particles in the unit cell

The unit-cell parameters together with the typical diameter of small RNA phages (280–300 Å) suggested that there are two particles in the asymmetric unit. Since in *P*1 one can choose the origin freely (the origin was chosen to be at the centre of one particle), there remain nine undetermined parameters: six parameters for the orientation of both particles and three for the relative position of the particle centres.

Reflections of type $h + k + l$ = odd were systematically weak at low resolution (to 7 Å) for both crystal forms *A* and *B*. This indicated that the cell is pseudo-*I*-centred and that both particles in the asymmetric unit must have similar orientations.

3.3. The rotation function

Although the space group is the same and the differences in unit-cell parameters are moderate, the particle orientations for the two crystal forms are completely different (Figs. 2*a* and 2*b*). Since there are two particles in the asymmetric unit in both cells, it was surprising that both of them seemed to have the same orientation, even if similar orientations were predicted from the systematically weak reflections of type $h + k + l$ = odd. However, when using only high-resolution reflections (5.5–4.3 Å for form *A* and 4.5–3.4 Å for form *B*) and a larger integration radius (200 Å), the peaks split clearly (Figs. 2*c*–2*g*). The importance of using thin resolution shells at the highest possible resolution to resolve similar particle orientations has been demonstrated previously (Muckelbauer *et al.*, 1995). The split peaks also show two extra peaks. The same appearance of this pattern of rotation-function peaks from particles with similar orientations has been observed previously (Oliveira *et al.*, 1993; Muckelbauer *et al.*, 1995; Wikoff *et al.*, 1999) and has been explained as packing peaks (Muckelbauer *et al.*, 1995). Packing peaks can be generated by the symmetry of the packing of particles in the crystal (Åkervall *et al.*, 1971), but it is not obvious what features of the packing would generate the observed pattern.

A locked self-rotation function (Rossmann *et al.*, 1972) was calculated on a coarse grid (5°) covering all three polar angles φ, ψ, κ for 0–180°. The highest peak was selected for a finer search (in 0.1° steps). The final locked rotation function showed clearly two closely located but separate peaks with an overlap peak in the middle (Figs. 3*a* and 3*b*). When a smaller integration radius (50 Å) was chosen, only one peak was found at a position between the two true peaks.

The final results showed that particle orientations relative to the standard icosahedral orientation are φ_{1b} = 140.4, ψ_{1b} = 70.4, κ_{1b} = 95.3, φ_{2b} = 140.2, ψ_{2b} = 69.5 and κ_{2b} = 96.3° for crystal form *B*, and φ_{1a} = 149.0, ψ_{1a} = 69.6, κ_{1a} = 149.6, φ_{2a} = 149.8, ψ_{2a} = 70.0 and κ_{2a} = 149.7° for crystal form *A*. The results from the locked self-rotation function in most cases matched exactly with the peaks in the self-rotation searches. In Fig. 4,

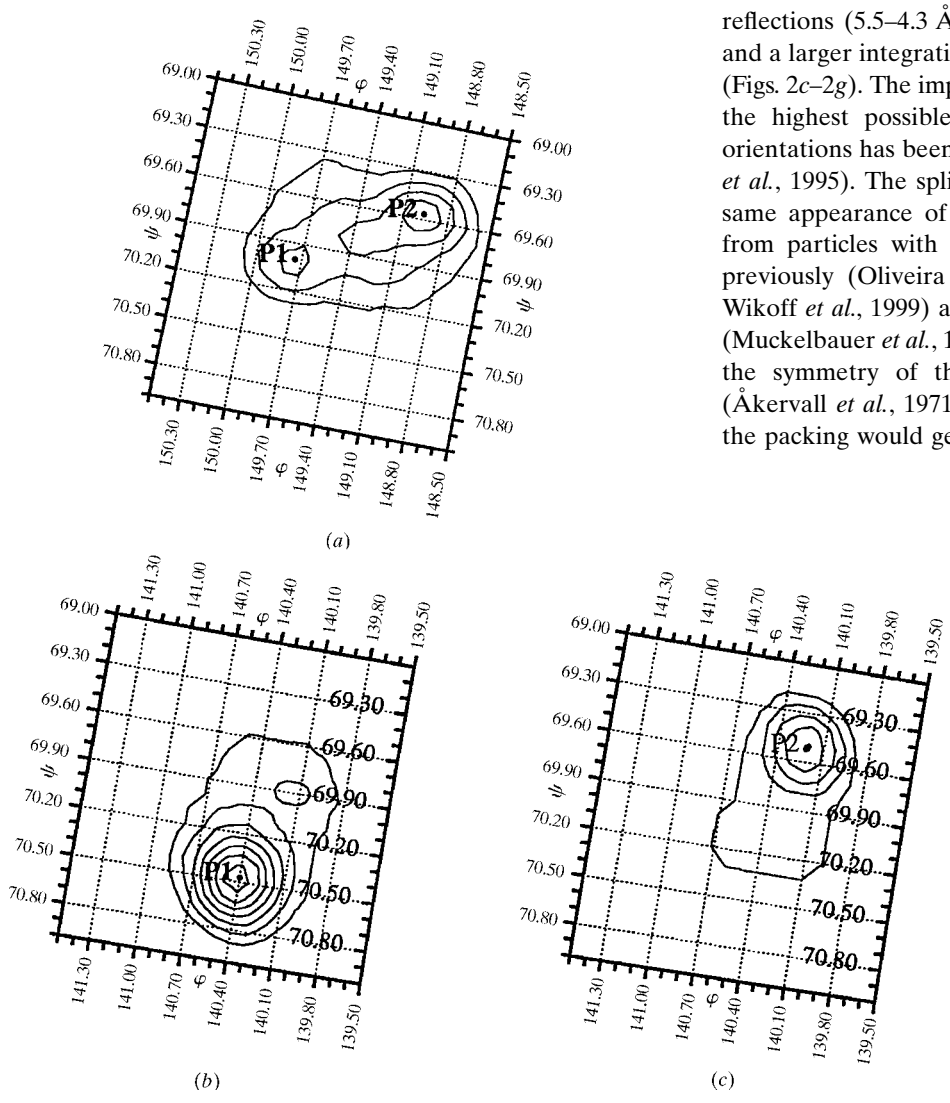

Figure 3
Detailed searches of the locked rotation functions of crystal forms *A* and *B*. (*a*) Crystal form *A*, κ = 149.6°, 5.5–4.4 Å resolution; for crystal form *B*, 4.5–3.4 Å resolution, two sections of (*b*) κ = 96.3° and (*c*) κ = 95.3° are displayed. In both cases, there are two peaks P1 and P2 corresponding to the orientations of the two particles. Between them there is an overlap peak, which can be regarded as an average of both true peaks. When a smaller radius of integration or lower resolution is used, only this average peak is seen.

Table 2
Scaling statistics for crystal forms *A* and *B*.

Crystal form *A*			Crystal form *B*		
Resolution	R_{merge}	Completeness	Resolution	R_{merge}	Completeness
200–11.40	0.113	39.1	200–14.76	0.170	54.8
9.05	0.140	45.3	10.45	0.175	60.0
7.90	0.179	45.3	8.54	0.201	63.7
7.18	0.225	43.6	7.40	0.240	63.4
6.67	0.236	38.4	6.62	0.292	61.7
6.27	0.267	33.2	6.04	0.379	58.9
5.96	0.328	31.7	5.59	0.377	57.4
5.70	0.323	30.5	5.23	0.364	56.1
5.48	0.316	30.1	4.93	0.418	54.0
5.29	0.288	28.6	4.68	0.376	51.9
5.13	0.331	28.3	4.46	0.407	46.5
4.98	0.322	27.2	4.27	0.426	39.2
4.85	0.327	25.7	4.11	0.461	28.7
4.73	0.296	24.6	3.96	0.427	19.0
4.62	0.262	21.9	3.82	0.518	11.3
4.52	0.313	19.1	3.70	0.488	6.8
4.43	0.331	14.6	3.59	0.553	5.7
4.35	0.348	9.1	3.49	0.682	4.0
4.27	0.361	5.2	3.40	0.782	1.7
All reflections	0.186	27.1	All reflections	0.270	30.0
Number of reflections	259624			606783	

† $R_{merge} = 100\sum_h \sum_j |I_{hj} - \langle I_h \rangle| / \sum\sum I_{hj}$.

the orientations of both particles for crystal form *B* are shown, as determined by the locked self-rotation function.

3.4. The Patterson function

In order to locate the position of the second particle, a native Patterson function was calculated. If the particles have similar orientation, a peak corresponding to the vector between them is expected. When using reflections in the resolution range 20–8 Å, a peak appeared at x = 154.9, y = 166.9, z = 189.6 Å for crystal form *B* and at x = 141.7, y = 162.4, z = 182.5 Å for crystal form *A* (orthogonal coordinates). In both cases, these peaks were at a level of 60% of the origin peak. The positions of the peaks correspond exactly to (0.5, 0.5, 0.5) in crystal coordinates. This position was expected from the unit-cell parameters and particle diameter. Since the peak is found at the inversion center of the Patterson function (space group $P\bar{1}$), a small deviation from this position is expected to be masked by overlap with the symmetry-related peak. The Patterson function was calculated using several resolution limits (20–9, 20–3.4, 8.0–3.4 and 12.0–6.0 Å) to test whether the peak had any tendency to move away from the inversion center. At 8.0–3.4 Å resolution, no significant peak except the origin peak was observed. This is most likely to be caused by the slightly different orientation of the two particles. When other resolution limits were used, the highest peak was always exactly at (0.5, 0.5, 0.5), but the height of the peak in relation to the origin peak was reduced when higher resolution data was used.

3.5. Phasing

Phasing was performed using the same protocol for both crystal forms. As the model for molecular replacement we used the protein shell of MS2 (PDB entry 2ms2), the structure of which had been determined previously (Valegård *et al.*, 1990). The MS2 coat protein has a sequence identity of about 10% to PP7, well below the level of identity required for molecular replacement at high resolution. Comparisons of the conformation of phage coat proteins suggest that the expected degree of structural similarity between the PP7 and MS2 coat proteins would correspond to an r.m.s. deviation of at best 2.5 Å for C^{α} atoms (Tars *et al.*, 1997).

From the unit-cell parameters, it was estimated that phage PP7 has a slightly larger diameter (about 7–10 Å) than MS2. A poly-alanine model of MS2 coordinates was made and the three subunits were moved individually by 7 Å in a direction radially away from the particle centre. The 120 non-crystallographic symmetry operators were generated using the icosahedral geometry and the orientation and position of both particles in the asymmetric unit. The initial phases were calculated in *X-PLOR* (Brünger, 1990). The initial R factor between the model and the observed amplitudes was 0.54 for reflections in the resolution range 20–10 Å.

A mask was created covering all model atoms with a sphere of 12 Å radius. A $2F_o - F_c$ map was calculated to 15 Å resolution using model phases and observed amplitudes. Real-space averaging was performed using the *RAVE* package (Kleywegt & Jones, 1993, 1994). In the presence of non-

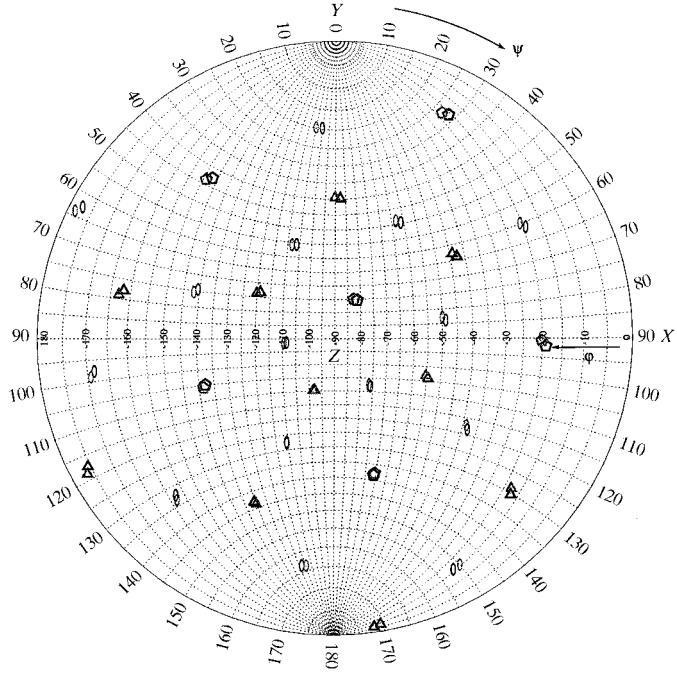

Figure 4
Particle orientations for crystal form *B* as determined by the locked self-rotation function at 4.5–3.4 Å resolution. The symbols for fivefold, threefold and twofold axes are drawn with solid and dashed lines for the two particles, respectively.

crystallographic symmetry, successful phase determination can also be performed with incomplete data. In this case, the data was about 30% complete and at the resolution edge used it was about 5% complete. Similar levels of completeness have been used in other virus structure determinations (Chandrasekar & Johnson, 1998; Tate *et al.*, 1999). Phase extension from 15 to 8 Å was performed in several steps, each step corresponding to extension by one reciprocal-space index in the *l* direction. For each extension cycle, four cycles of averaging were performed. Missing reflections were not replaced by calculated values during the phase extension. The map was examined at this stage and showed clearly the expected density of PP7, but shifted by about 3 Å outwards compared with the model. The model subunits were manually fitted as rigid bodies into the density where the β-sheet and helices appeared clearly. Phases from the new model were calculated in *X-PLOR*. The *R* factor remained at 0.54. The averaging and phase extension was repeated, this time in the resolution range 15–3.7 Å (15–4.4 Å for crystal form *A*). Inspection of the map showed that some parts of the electron density (particularly covering the FG loop of the B subunit) might be outside the mask. The mask was then manually corrected in the program *O* (Jones *et al.*, 1990) and ten further averaging cycles at 3.7 Å resolution were run using the new mask.

For both crystal forms, the map looked very similar, in spite of the resolution for crystal form *B* being higher. The data in the resolution range 4.5–3.4 Å is limited and of poor quality as judged by the scaling statistics. This data still contains some useful information, since the rotation function for crystal form *B* and data in the resolution range 4.5–3.4 Å gave clear peaks corresponding to the icosahedral symmetry elements. The data at low resolution might contain severe errors, as suggested by the complex diffraction pattern at low resolution, the serious problems with data processing and the poor scaling statistics. To test if the 'high' resolution data could be useful, another map was calculated and averaged for ten cycles, using only data in the resolution range 7–3.7 Å. This gave a significant improvement in the map quality (Fig. 5) in all parts of the model except at the more disordered C-terminus, where the original map was slightly better. The new map obtained from crystal form *B* was much better than that from crystal form *A*. The map from crystal form *A* did not represent any features which were lacking in the crystal form *B* map. Therefore, multi-crystal averaging was not attempted. Subsequently, only the map of crystal form *B* was used for model building and refinement.

Since the Patterson function was calculated using the low-resolution data only, the centre of the second particle might not be defined with sufficient precision. An improved position was determined by shifting the particle centre and monitoring the correlation coefficient in averaging. A program was written which automatically performed this operation. The algorithm for this is shown in Fig. 6. Four cycles of averaging were run for each new position. The initial step size was 2 Å. Since no improvement was achieved (correlation coefficient was worse than 0.4 in most cases), further step sizes of 1, 0.5, 0.25 and 0.125 Å were tried. The best correlation coefficient was obtained with a minor shift of the second particle by $\Delta x = -0.25$ Å. This improved the correlation coefficient for reflections between 7 and 3.7 Å resolution from 0.667 to 0.671. In all other calculated positions, the correlation coefficient was worse than 0.667. The correlation coefficient dropped to less than 0.40 if the particle was moved for more than 2 Å in any direction and to less than 0.60 if moved for more than 1 Å. According to our calculations, the particle centre is defined within an error of less than 0.2 Å.

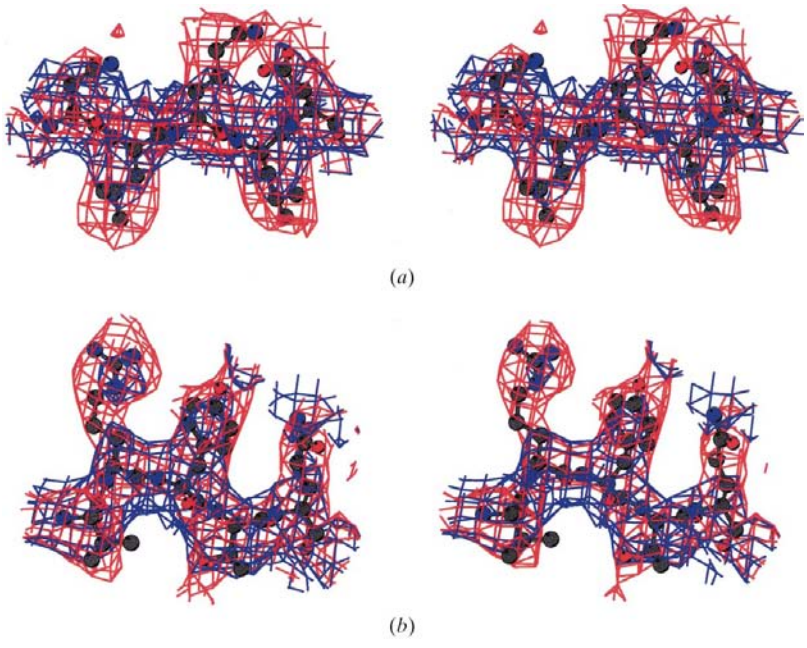

Figure 5
Comparison of two electron-density maps for crystal form *B*, calculated at 20–3.7 Å resolution (blue) and 7–3.7 Å resolution (red), contoured at the same σ levels. Two regions of model are shown in stereo. (*a*) Residues B56–B60. There is density for a salt bridge between Arg58 and GluB60, which cannot be observed at any contouring level when using all the data from 20 to 3.7 Å. (*b*) Residues C78–C82.

3.6. Model building and refinement

The amino-acid sequence of PP7 could easily be fitted to the side-chain density in the map. Owing to the low resolution, however, several side chains were not visible, especially in the loop regions.

The PP7 model was built manually in program *O* using the modified MS2 model as a starting point.

The structure was refined with the conjugate-gradient method, followed by simulated annealing in *CNS* (Brunger *et al.*, 1998). Strict icosahedral constraints and positional refinement were used. The *R* factor fell from 0.49 (after map calculation, using the built PP7 model) to 0.41 after conjugate gradient and 0.35 after simulated annealing. The model was inspected and outliers

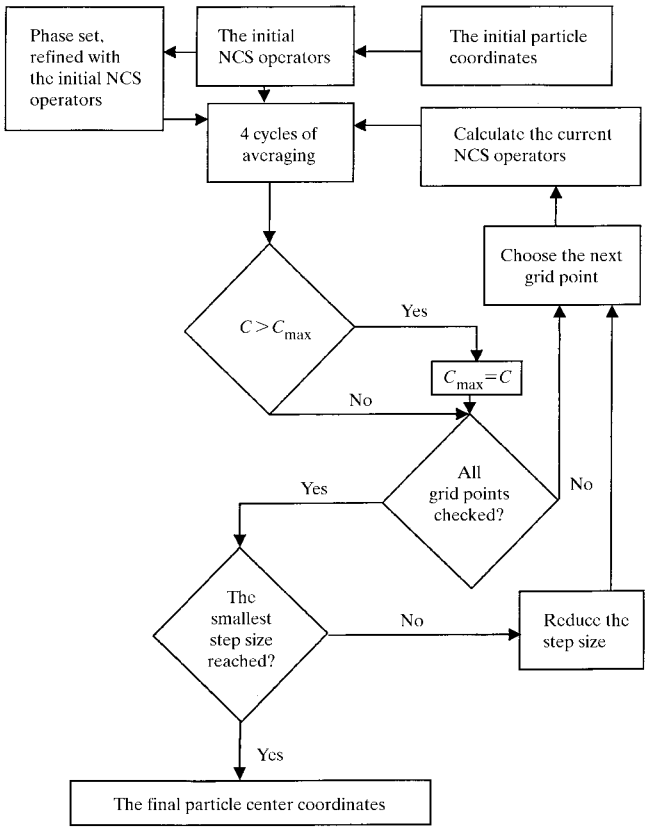

Figure 6
The general algorithm for refinement of the second particle centre. The particle was moved around in all three directions, which means that for each grid point (corresponding to the current best particle position) all 26 neighbouring grid points were checked. For each new particle position, four cycles of averaging were performed. An average correlation coefficient for higher resolution bins (7–3.7 Å) was calculated. If the central grid point gave the best results, the step size was reduced by a factor of two and the whole process was repeated.

in the Ramachandran plot were corrected whenever possible. This was followed by one further conjugate-gradient refinement. The Ramachandran plot for the final model had 5% outliers as defined by Kleywegt & Jones (1996). The present R factor is 0.34 for all reflections.

This work was supported by the Swedish Natural Science Research Council, by the Royal Swedish Academy of Sciences and by the Latvian Science Council. We thank C. Helgstrand and E. Grahn for help with data collection. We also thank Dr A. Dishler and Dr L. Orna for qualified technical support. The PP7 phage was kindly supplied by Dr J. van Duin, Leiden University.

References

Acharya, K. R., Fry, E., Stuart, D., Fox, G., Rowlands, D. & Brown, F. (1989). *Nature (London)*, **337**, 709–716.
Åkervall, K., Strandberg, B., Rossmann, M. G., Bengtsson, U., Fridborg, K., Johannisen, H., Kannan, K. K., Lövgren, S., Petef, G., Öberg, B., Eaker, D., Hjertén, S., Rydén, L. & Moring, I. (1971). *Cold Spring Harbor Symp. Quant. Biol.* **36**, 469–488.
Brünger, A. T. (1990). *X-PLOR Manual*. New Haven, CT, USA: Yale University Press.
Brunger, A. T., Adams, P. D., Clore, G. M., DeLano, W. L., Gros, P., Grosse-Kunstleve, R. W., Jiang, J.-S., Kuszewski, J., Nilges, M., Pannu, N. S., Read, R. J., Rice, L. M., Simonson, T. & Warren, G. L. (1998). *Acta Cryst.* D**54**, 905–921.
Chandrasekar, V. & Johnson, J. E. (1998). *Structure*, **6**, 157–171.
Collaborative Computational Project, Number 4 (1994). *Acta Cryst.* D**50**, 760–763.
Dokland, T., McKenna, R., Sherman, D. M., Bowman, B. R., Bean, W. F. & Rossmann, M. G. (1998). *Acta Cryst.* D**54**, 878–890.
Golmohammadi, R., Fridborg, K., Bundule, M., Valegård, K. & Liljas, L. (1996). *Structure*, **4**, 543–554.
Golmohammadi, R., Valegård, K., Fridborg, K. & Liljas, L. (1993). *J. Mol. Biol.* **234**, 620–639.
Hogle, J. M., Chow, M. & Filman, D. J. (1985). *Science*, **229**, 1358–1365.
Hogle, J. M., Maeda, A. & Harrison, S. C. (1986). *J. Mol. Biol.* **191**, 625–638.
Jones, T. A., Bergdoll, M. & Kjeldgaard, M. (1990). *Crystallographic and Modeling Methods in Molecular Design*, edited by C. Bugg & S. Ealick, pp. 189–199. New York: Springer–Verlag.
Kleywegt, G. J. & Jones, T. A. (1993). *CCP4/ESF–EACBM Newslett. Protein Crystallogr.* **29**, 56–59.
Kleywegt, G. J. & Jones, T. A. (1994). *Proceedings of the CCP4 Study Weekend. From First Map to Final Model*, edited by S. Bailey, R. Hubbard & D. Waller, pp. 59–66. Warrington: Daresbury Laboratory.
Kleywegt, G. J. & Jones, T. A. (1996). *Structure*, **4**, 1395–1400.
Luo, M., Vriend, G., Kamer, K., Minor, I., Arnold, E., Rossmann, M. G., Boege, U., Scraba, D. G., Duke, G. M. & Palmenberg, A. C. (1987). *Science*, **235**, 182–191.
McKenna, R., Xia, D., Willingmann, P., Ilag, L. L. & Rossmann, M. G. (1992). *Acta Cryst.* B**48**, 499–511.
Muckelbauer, J. K., Kremer, M., Minor, I., Tong, L., Zlotnick, A., Johnson, J. E. & Rossmann, M. G. (1995). *Acta Cryst.* D**51**, 871–887.
Munshi, S., Liljas, L. & Johnson, J. E. (1998). *Acta Cryst.* D**54**, 1295–1305.
Oliveira, M. A., Zhao, R., Lee, W.-M., Kremer, M. J., Minor, I., Rueckert, R. R., Diana, G. D., Pevear, D. C., Dutko, F. J., McKinlay, M. A. & Rossmann, M. G. (1993). *Structure*, **1**, 51–68.
Olsthoorn, R. C. L., Garde, G., Dayhuff, T., Atkins, J. F. & van Duin, J. (1995). *Virology*, **206**, 611–625.
Otwinowski, Z. & Minor, W. (1996). *Methods Enzymol.* **276**, 307–326.
Rossmann, M. G., Arnold, E., Erickson, J. W., Frankenberger, E. A., Griffith, J. P., Hecht, H.-J., Johnson, J. E., Kamer, G., Luo, M., Mosser, A. G., Rueckert, R. R., Sherry, B. & Vriend, G. (1985). *Nature (London)*, **317**, 145–153.
Rossmann, M. G. & Blow, D. M. (1962). *Acta Cryst.* **15**, 24–31.
Rossmann, M. G., Ford, G. C., Watson, H. C. & Banaszak, L. J. (1972). *J. Mol. Biol.* **64**, 237–249.
Simpson, A. A., Chipman, P. R., Baker, T. S., Tijssen, P. & Rossmann, M. G. (1998). *Structure*, **6**, 1355–1367.
Speir, J. A., Munshi, S., Wang, G., Baker, T. S. & Johnson, J. E. (1995). *Structure*, **3**, 63–78.
Tars, K., Bundule, M., Fridborg, K. & Liljas, L. (1997). *J. Mol. Biol.* **271**, 759–773.
Tate, J., Liljas, L., Christian, P., Lin, T., Scotti, P. & Johnson, J. E. (1999). *Nature Struct. Biol.* **6**, 765–774.
Tong, L. & Rossmann, M. G. (1990). *Acta Cryst.* A**46**, 783–792.
Valegård, K., Liljas, L., Fridborg, K. & Unge, T. (1990). *Nature (London)*, **345**, 36–41.
Valegård, K., Liljas, L., Fridborg, K. & Unge, T. (1991). *Acta Cryst.* B**47**, 949–960.
Wikoff, W. R., Duda, R. L., Hendrix, R. H. & Johnson, J. E. (1999). *Acta Cryst.* D**55**, 763–771.